Journal of Sound and Vibration (1998) **217**(3), 435–452
Article No. sv981782

STABILITY ANALYSIS OF A CIRCULARLY TOWED CABLE–BODY SYSTEM

F. Zhu and C. D. Rahn

Department of Mechanical Engineering, *Clemson University*, *Clemson*, *SC* 29634, *U.S.A.*

(*Received* 4 *April* 1997, *and in final form* 18 *May* 1998)

This paper investigates the dynamic response of a circularly towed cable–body system with fluid drag loading. The system model includes non-linear steady state equations and linear vibrational equations about steady state. The steady state equations are solved numerically via a shooting technique. The vibrational equations are linearized and discretized using Galerkin's method. Numerical results show the existence of multiple steady state solutions for small fluid drag, large end mass, or high rotation speed. Divergently unstable solutions lead to jump phenomena. High rotation speed causes Hopf bifurcations and second mode flutter for small point mass radius or third mode flutter for large point mass radius. Generally, increasing drag increases the stable regions. Stable single-valued solutions always exist for sufficiently low rotation speed.

1. INTRODUCTION

Circularly towed cable systems have been studied for more than half a century because of applications in air and marine towed vehicles and their fascinating dynamic response. Caughey [1] presented an approximate analysis of a whirling heavy chain in a vacuum, including the whirling mode stability. He noticed the similarity of the response to that of a hardening spring–mass system. Huang [2] predicted the existence of multi-valued equilibrium solutions for a cable towed by an orbiting aircraft in air. Skop and Choo [3] derived the equilibrium equations of a steadily moving cable–body system and numerically investigated the multi-valued regions. For a cable towed in water, however, Choo and Casarella [4] found only single-valued solutions.

The stability of circularly towed cable–body systems was later studied qualitatively by Russell and Anderson based on a simplified two-degree-of-freedom lumped-mass model [5]. In reference [6], a finite element model for linear displacement from the steady state equilibrium quantitatively predicted static instability, jump phenomena, and dynamic instability of a continuous cable–body system. Good agreement between numerical and experimental results were detailed in references [6] and [7].

Zhu *et al*. [8] recently studied the steady state response and stability of an extensible string fixed at one boundary and undergoing constant speed circular

0022–460X/98/430435 + 18 $30.00/0

motion at the other boundary. The influence of air drag on ballooning strings was also investigated [9]. In these papers, divergent and flutter instabilities were predicted and verified experimentally.

The dynamics of the circularly towed cable–body system is re-investigated in this paper using an approach different from that of reference [6]. Based on Newton's law, the steady state and perturbed vibration equations are derived. The steady state equations are solved numerically via a shooting method and the perturbed vibrational equations are approximated using Galerkin's approach. The effects of various parameters on the steady state solutions and their stability are discussed. Some results are compared qualitatively with Russell and Anderson's experiment in references [6] and [7].

2. EQUATIONS OF MOTION

Figure 1 shows a schematic diagram of the towed cable–body system. A cable of length L undergoes constant speed circular motion Ω at the top boundary (e.g., attached to a ship or plane) and attaches to a point mass at the bottom (e.g., towed vehicle or payload). The radius of the circular path is denoted as a. The Cartesian co-ordinate system axes $\mathbf{i}$, $\mathbf{j}$, and $\mathbf{k}$ rotate at Ω about $\mathbf{k}$. The co-ordinates are chosen to align the steady state point mass position with the X-axis. Thus, X_d represents the radius of the steady state point mass motion. The vertical distance between the two ends of the cable is denoted by H.

The vector $\mathbf{R}_1(S_0) = X(S_0)\mathbf{i} + Y(S_0)\mathbf{j} + Z(S_0)\mathbf{k}$ locates the steady state configuration where S_0 is the unstressed arc length co-ordinate measured from the point mass. The perturbed configuration is located by $\mathbf{R}_2(S_0, T)$ with T the time. The relative displacement between these two configurations is

$$\mathbf{U}(S_0, T) = \mathbf{R}_2 - \mathbf{R}_1 = U_1\mathbf{i} + U_2\mathbf{j} + U_3\mathbf{k}. \tag{1}$$

By definition, the strains in the cable are

$$\epsilon_i = \frac{\partial S_i}{\partial S_0} - 1, \tag{2}$$

where $i = 1$ or 2 for the steady state and perturbed configurations, respectively, and S_i is the corresponding arc length co-ordinate. Lagrangian strains are

$$\epsilon_i = \frac{1}{2}\left(\frac{\partial \mathbf{R}_i}{\partial S_0} \cdot \frac{\partial \mathbf{R}_i}{\partial S_0} - 1\right). \tag{3}$$

The tension vectors are tangent to the cable,

$$\mathbf{P}_i = P_i \frac{\partial \mathbf{R}_i}{\partial S_0}\left(\frac{\partial S_i}{\partial S_0}\right)^{-1}, \tag{4}$$

and for a linearly elastic material,

$$P_i = EA_0\epsilon_i, \tag{5}$$

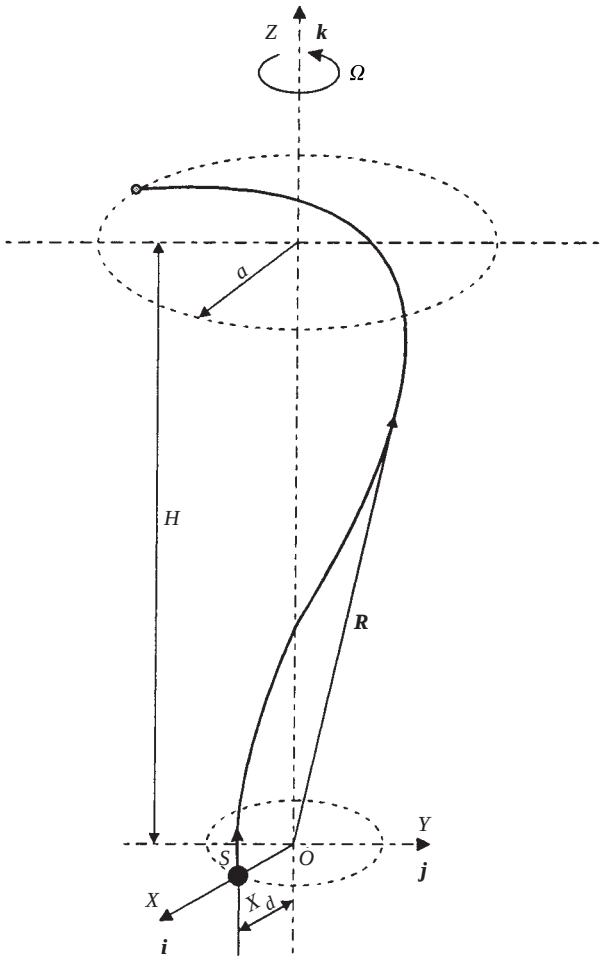

Figure 1. Schematic diagram of a circularly towed cable–body system.

where E is Young's modulus and A_0 is the cross-sectional area of the unstressed cable. Substitution of equations (5) and (2) into equation (4) gives

$$\mathbf{P}_2 = \frac{P_1\epsilon_2}{\epsilon_1(1+\epsilon_2)}\frac{\partial \mathbf{R}_2}{\partial S_0}. \tag{6}$$

The strains are assumed small so that $1 + \epsilon_i \approx 1$. Based on Newton's law, the cable's equation of motion is

$$\frac{\partial \mathbf{P}_2}{\partial S_0} + \mathbf{F}_w + \mathbf{F}_I + \mathbf{F}_D = 0, \tag{7}$$

where the gravitational force, inertial force, and normal hydraulic drag, respectively, are

$$\mathbf{F}_w = -\rho_b A_0 g \mathbf{k}, \tag{8}$$

$$\mathbf{F}_I = -\rho_a A_0 \left\{ \Omega^2 \mathbf{k} \times (\mathbf{k} \times \mathbf{R}_1) + \Omega^2 \mathbf{k} \times (\mathbf{k} \times \mathbf{U}) + 2\Omega \mathbf{k} \times \frac{\partial \mathbf{U}}{\partial T} + \frac{\partial^2 \mathbf{U}}{\partial T^2} \right\}, \tag{9}$$

$$\mathbf{F}_D = -D_n |\mathbf{V}_n^f| \mathbf{V}_n^f. \tag{10}$$

The cable mass densities ρ_b and ρ_a include buoyancy and added mass from the fluid, respectively. D_n is the drag coefficient and $\mathbf{V}_n^f$ is the normal velocity given by

$$\mathbf{V}_n^f = \frac{\partial \mathbf{R}_2}{\partial S_0} \times \left(\left(\frac{\partial \mathbf{U}}{\partial T} + \Omega \mathbf{k} \times (\mathbf{U} + \mathbf{R}_1) \right) \times \frac{\partial \mathbf{R}_2}{\partial S_0} \right). \tag{11}$$

The tangential drag component is assumed negligibly small to simplify analysis. Russell and Anderson [6] included tangential drag in their model and obtained good agreement with experiments. The tangential drag coefficient, however, was less than 3% of the normal drag coefficient. A good match between the theory and experiment was also obtained for rotating strings with fixed ends by neglecting the tangential drag component [9].

Substitution of equations (1), (6), and (8)–(10) into equation (7) with the small strain assumption and rearrangement yields

$$\begin{aligned} &\frac{\partial}{\partial S_0} \left(\frac{P_1 \epsilon_2}{\epsilon_1} \left(\frac{\partial \mathbf{R}_1}{\partial S_0} + \frac{\partial \mathbf{U}}{\partial S_0} \right) \right) \\ &\quad = \rho_a A_0 \left\{ \Omega^2 \mathbf{k} \times (\mathbf{k} \times \mathbf{R}_1) + \Omega^2 \mathbf{k} \times (\mathbf{k} \times \mathbf{U}) + 2\Omega \mathbf{k} \times \frac{\partial \mathbf{U}}{\partial T} + \frac{\partial^2 \mathbf{U}}{\partial T^2} \right\} \\ &\qquad + \rho_b A_0 g \mathbf{k} + D_n |\mathbf{V}_n^f| \mathbf{V}_n^f. \end{aligned} \tag{12}$$

Non-dimensionization produces

$$\begin{aligned} &\frac{\partial}{\partial s} \left(\frac{p \epsilon_2}{\epsilon_1} \left(\frac{\partial \mathbf{r}}{\partial s} + \frac{\partial \mathbf{u}}{\partial s} \right) \right) \\ &\quad = \rho \mathbf{k} + \omega^2 \left[\mathbf{k} \times (\mathbf{k} \times \mathbf{r}) + \mathbf{k} \times (\mathbf{k} \times \mathbf{u}) + 2\mathbf{k} \times \frac{\partial \mathbf{u}}{\partial t} + \frac{\partial^2 \mathbf{u}}{\partial t^2} + d_n |\mathbf{v}_n^f| \mathbf{v}_n^f \right], \end{aligned} \tag{13}$$

where

$$\mathbf{r} = x\mathbf{i} + y\mathbf{j} + z\mathbf{k} = \frac{\mathbf{R}_1}{a}, \qquad s = \frac{S_0}{a}, \qquad \mathbf{u} = \frac{\mathbf{U}}{a}, \qquad t = \Omega T, \tag{14}$$

$$\omega^2 = \frac{a\Omega^2}{g}, \qquad \rho = \frac{\rho_b}{\rho_a}, \qquad d_n = \frac{D_n}{\rho_a A_0}, \qquad p = \frac{P_1}{\rho_a A_0 a g}, \qquad \gamma = \frac{E}{\rho_a a g}, \tag{15}$$

$$\epsilon_1 = \frac{p}{\gamma}, \qquad \epsilon_2 = \epsilon_1 + \frac{\partial \mathbf{r}}{\partial s} \cdot \frac{\partial \mathbf{u}}{\partial s} + \frac{1}{2} \frac{\partial \mathbf{u}}{\partial s} \cdot \frac{\partial \mathbf{u}}{\partial s}, \tag{16}$$

$$\mathbf{v}_n^f = \frac{\partial(\mathbf{r}+\mathbf{u})}{\partial s} \times \left(\left(\frac{\partial \mathbf{u}}{\partial t} + \mathbf{k} \times (\mathbf{u}+\mathbf{r}) \right) \times \frac{\partial(\mathbf{r}+\mathbf{u})}{\partial s} \right). \tag{17}$$

The second equation of equations (16) is obtained by using equation (3).

The natural boundary condition associated with the point mass is

$$\mathbf{P}_2 + \mathbf{F}_{dw} + \mathbf{F}_{dI} + \mathbf{F}_{dH} = 0, \tag{18}$$

where the point mass net weight in the fluid, inertial force and fluid drag are, respectively,

$$\mathbf{F}_{dw} = -W\mathbf{k}, \tag{19}$$

$$\mathbf{F}_{dI} = -M\left(\Omega^2 \mathbf{k} \times (\mathbf{k} \times \mathbf{R}_1) + \Omega^2 \mathbf{k} \times (\mathbf{k} \times \mathbf{U}_d) + 2\Omega \mathbf{k} \times \frac{\partial \mathbf{U}_d}{\partial T} + \frac{\partial^2 \mathbf{U}_d}{\partial T^2} \right), \tag{20}$$

$$\mathbf{F}_{dH} = -D\left| \frac{\partial \mathbf{U}_d}{\partial T} + \Omega \mathbf{k} \times (\mathbf{U}_d + \mathbf{R}_1) \right| \left(\frac{\partial \mathbf{U}_d}{\partial T} + \Omega \mathbf{k} \times (\mathbf{U}_d + \mathbf{R}_1) \right). \tag{21}$$

where $\mathbf{U}_d = \mathbf{U}(0,t)$. The weight (including buoyancy), mass (including added mass), and fluid drag coefficient of the point mass are W, M, and D, respectively.

Substitution of equations (6) and (19)–(21) into equation (18) and non-dimensionalization gives

$$\begin{aligned} &\frac{p_d \epsilon_2}{\epsilon_1} \left(\frac{\partial \mathbf{r}}{\partial s} + \frac{\partial \mathbf{u}_d}{\partial s} \right) \\ &\quad = w\mathbf{k} + m\omega^2 \left(\mathbf{k} \times (\mathbf{k} \times \mathbf{r}) + \mathbf{k} \times (\mathbf{k} \times \mathbf{u}_d) + 2\mathbf{k} \times \frac{\partial \mathbf{u}_d}{\partial t} + \frac{\partial^2 \mathbf{u}_d}{\partial t^2} \right) \\ &\quad + \mathrm{d}\omega^2 \left| \frac{\partial \mathbf{u}_d}{\partial t} + \mathbf{k} \times (\mathbf{u}_d + \mathbf{r}) \right| \left(\frac{\partial \mathbf{u}_d}{\partial t} + \mathbf{k} \times (\mathbf{u}_d + \mathbf{r}) \right), \end{aligned} \tag{22}$$

where p_d is the cable tension at $s = 0$,

$$w = \frac{W}{\rho_a a A_0 g}, \qquad m = \frac{M}{\rho_a a A_0}, \qquad d = \frac{D}{\rho_a A_0}, \qquad \text{and} \qquad \mathbf{u}_d = \frac{\mathbf{U}_d}{a}. \tag{23}$$

The following boundary conditions complete the model:

$$x = X_d/a = x_d, \qquad y = z = 0, \qquad \text{at} \qquad s = 0, \tag{24}$$

$$x^2 + y^2 = 1, \qquad \mathbf{u} = 0, \qquad \text{at} \qquad s = L/a = l. \tag{25}$$

3. STEADY STATE SOLUTIONS

In steady state, the displacement $\mathbf{u} = \mathbf{0}$, so equation (13) simplifies to

$$\frac{\mathrm{d}}{\mathrm{d}s}\left(p\,\frac{\mathrm{d}\mathbf{r}}{\mathrm{d}s}\right) = \rho\mathbf{k} + \omega^2[\mathbf{k}\times(\mathbf{k}\times\mathbf{r}) + d_n|\mathbf{v}_n^i|\mathbf{v}_n^i], \tag{26}$$

where

$$\mathbf{v}_n^i = \frac{\mathrm{d}\mathbf{r}}{\mathrm{d}s}\times\left((\mathbf{k}\times\mathbf{r})\times\frac{\mathrm{d}\mathbf{r}}{\mathrm{d}s}\right). \tag{27}$$

The elasticity parameter γ does not appear in equation (26) because the small strain assumption neglects the cable extension. Zhu *et al*. [8] discussed the effect of extensibility on a similar rotating system.

The steady state point mass equation is

$$p_d\frac{\mathrm{d}\mathbf{r}}{\mathrm{d}s} = w\mathbf{k} + m\omega^2\mathbf{k}\times(\mathbf{k}\times\mathbf{r}) + \mathrm{d}\omega^2|\mathbf{k}\times\mathbf{r}|(\mathbf{k}\times\mathbf{r}). \tag{28}$$

Equation (28) contains three scalar equations:

$$\frac{\mathrm{d}x}{\mathrm{d}s} = -\omega^2\frac{mx_d}{p_d}, \qquad \frac{\mathrm{d}y}{\mathrm{d}s} = \mathrm{d}\omega^2\frac{x_d^2}{p_d}, \qquad \frac{\mathrm{d}z}{\mathrm{d}s} = \frac{w}{p_d}. \tag{29–31}$$

The square sum of these equations gives

$$p_d = \omega^2\sqrt{m^2x_d^2 + (\mathrm{d}x_d^2)^2 + \left(\frac{w}{\omega^2}\right)^2}. \tag{32}$$

Similarly, the scalar equations in equation (26) are

$$px_{,ss} = -p_{,s}x_{,s} + \omega^2\{-x - d_n|\mathbf{v}_n^i|[y - x_{,s}(yx_{,s} - y_{,s}x)]\}, \tag{33}$$

$$py_{,ss} = -p_{,s}y_{,s} + \omega^2\{-y + d_n|\mathbf{v}_n^i|[x - y_{,s}(xy_{,s} - x_{,s}y)]\}, \tag{34}$$

$$pz_{,ss} = \rho - p_{,s}z_{,s} + \omega^2 d_n|\mathbf{v}_n^i|[z_{,s}(yx_{,s} - y_{,s}x)], \tag{35}$$

where $(\,\cdot\,)_{,s} = \mathrm{d}(\,\cdot\,)/\mathrm{d}s$ and

$$|\mathbf{v}_n^i| = [z_{,s}^2(x^2 + y^2) + (xx_{,s} + yy_{,s})^2]^{1/2}. \tag{36}$$

Dot multiplication of equation (26) and application of the relations

$$\frac{\mathrm{d}\mathbf{r}}{\mathrm{d}s}\cdot\frac{\mathrm{d}\mathbf{r}}{\mathrm{d}s} = 1, \qquad \frac{\mathrm{d}\mathbf{r}}{\mathrm{d}s}\cdot\frac{\mathrm{d}^2\mathbf{r}}{\mathrm{d}s^2} = 0, \qquad \frac{\mathrm{d}\mathbf{r}}{\mathrm{d}s}\cdot\mathbf{v}_n^i = 0,$$

$$\frac{\mathrm{d}\mathbf{r}}{\mathrm{d}s}\cdot(\mathbf{k}\times(\mathbf{k}\times\mathbf{r})) = -\frac{1}{2}\frac{\mathrm{d}}{\mathrm{d}s}(x^2 + y^2), \qquad \frac{\mathrm{d}\mathbf{r}}{\mathrm{d}s}\cdot\rho\mathbf{k} = \frac{\mathrm{d}}{\mathrm{d}s}(\rho z),$$

gives the steady state cable tension

$$p = p_d + \rho z + \frac{\omega^2}{2}(x_d^2 - x^2 - y^2). \tag{37}$$

Note that the simple, closed form expression for tension in equation (37) results from neglect of the tangential air drag.

For the simple case of a neutrally bouyant cable without drag (i.e., $\rho = 0$, and $d_n = d = 0$), the steady state solution is planar and can be solved exactly using Jacobian elliptical sine functions (see Appendix A). In general, however, the steady state solution is not planar and the non-linear differential equations (33)–(35) are solved numerically via a shooting technique. A Runge–Kutta fourth order integrator integrates the equations from $s = 0$ until $s = l$. Equations (24) and (29)–(31) provide six initial conditions with x_d as an initial guessed value. The value of x_d that minimizes the error, $x(l)^2 + y(l)^2 - 1$, is determined using an optimization algorithm in MATLAB. Using a wide range of initial values for x_d ensures discovery of multiple solutions.

4. LINEARIZED EQUATION OF VIBRATION

Substitution of equation (16) into equation (13), elimination of the non-linear $\mathbf{u}(s, t)$ terms, and cancellation of the steady state terms results in the linearized vibration equation,

$$\frac{\partial}{\partial s}\left[\gamma\left(\frac{\partial \mathbf{r}}{\partial s}\cdot\frac{\partial \mathbf{u}}{\partial s}\right)\frac{\partial \mathbf{r}}{\partial s} + p\,\frac{\partial \mathbf{u}}{\partial s}\right]$$

$$= \omega^2\left\{\mathbf{k}\times(\mathbf{k}\times\mathbf{u}) + 2\mathbf{k}\times\frac{\partial \mathbf{u}}{\partial t} + \frac{\partial^2 \mathbf{u}}{\partial t^2} + d_n\mathbf{J}\mathbf{v}_n\right\}. \tag{38}$$

Similarly, equation (22) linearizes to

$$\gamma\left(\frac{\partial \mathbf{r}}{\partial s}\cdot\frac{\partial \mathbf{u}_d}{\partial s}\right)\frac{\partial \mathbf{r}}{\partial s} + p_d\,\frac{\partial \mathbf{u}_d}{\partial s}$$

$$= m\omega^2\left(\mathbf{k}\times(\mathbf{k}\times\mathbf{u}_d) + 2\mathbf{k}\times\frac{\partial \mathbf{u}_d}{\partial t} + \frac{\partial^2 \mathbf{u}_d}{\partial t^2}\right) + \mathrm{d}\omega^2\mathbf{J}_d\left(\frac{\partial \mathbf{u}_d}{\partial t} + \mathbf{k}\times\mathbf{u}_d\right), \tag{39}$$

where the Jacobian matrices $\mathbf{J}$ and $\mathbf{J}_d$ are given in Appendix B.

Rewriting equations (38) and (39) in operator form yields

$$\begin{bmatrix}\mathbf{I} & \mathbf{0}\\ \mathbf{0} & \mathbf{I}\end{bmatrix}\begin{Bmatrix}\ddot{\mathbf{u}}\\ \ddot{\mathbf{u}}_d\end{Bmatrix} + \begin{bmatrix}\mathbf{G} & \mathbf{0}\\ \mathbf{0} & \mathbf{G}_d\end{bmatrix}\begin{Bmatrix}\dot{\mathbf{u}}\\ \dot{\mathbf{u}}_d\end{Bmatrix} + \begin{bmatrix}\mathbf{K} & \mathbf{0}\\ \mathbf{0} & \mathbf{K}_d\end{bmatrix}\begin{Bmatrix}\mathbf{u}\\ \mathbf{u}_d\end{Bmatrix} = \mathbf{0}, \tag{40}$$

where the matrix operators are defined in Appendix C.

Galerkin's method is used for numerical stability analysis. The displacement field is represented by an N-term separable series of the form

$$u_k(s, t) = \sum_{j=1}^{N} \eta_{jk}(t)\theta_j(s) \qquad (k = 1, 2, 3), \tag{41}$$

where the comparison functions are

$$\theta_j(s) = \sin(\beta_j(l-s)/l), \tag{42}$$

and β_j is the natural frequency of a string with one end fixed and the other end attached to a mass (see Appendix D). Substitution of equation (41) into equation (40) and application of Galerkin's method provides the discretized equation

$$\underline{\mathbf{M}}\ddot{\underline{\eta}} + \underline{\mathbf{G}}\dot{\underline{\eta}} + \underline{\mathbf{K}}\underline{\eta} = \underline{\mathbf{0}}, \tag{43}$$

with $\underline{\eta} = [\eta_{11}, \eta_{12}, \eta_{13}, \eta_{21}, \ldots, \eta_{N3}]^T$.

The eigenvalues (λ) of

$$\mathbf{A} = \begin{bmatrix} \underline{\mathbf{0}} & \underline{\mathbf{M}} \\ -\underline{\mathbf{K}} & -\underline{\mathbf{G}} \end{bmatrix}$$

are determined using MATLAB. The matrices $\underline{\mathbf{K}}$ and $\underline{\mathbf{G}}$ depend on the associated steady state configuration. Stable steady state solutions have eigenvalues with negative real parts. Eigenvalues with positive real parts and non-zero imaginary parts signify flutter (or dynamic) instability. A positive real eigenvalue indicates divergent instability.

5. NUMERICAL RESULTS

The non-dimensional cable equation (13) and point mass equation (22) depend on five (ω, ρ, d_n, γ, and l) and three (w, m, and d) parameters, respectively. In this paper, the effects of non-dimensional rotation speed (ω), cable fluid drag (d_n), cable length (l), and point mass (m) are investigated. Throughout the calculation, $\gamma = 600$, $N = 8$, and $d = 0{\cdot}1d_n$ are used. In addition, the fluid mass density is assumed to be negligibly small relative to the cable and point mass so $\rho = 1$ and $m = w$.

5.1. FLUID DRAG EFFECT

First, the effect of fluid drag on the steady state solutions and their dynamic stability is investigated. The non-dimensional parameters are $l = 3$, $\gamma = 600$, and $m = 3{\cdot}5$.

The solution curves of the verticality $v = h/l$ versus the rotation speed ω are plotted in Figure 2(a) for $d_n = 0{\cdot}8$, 1, 2, and 6. At low rotation speed, only one solution exists. When $\omega > 1$, multiple solutions are found for low drag values. As drag increases, the peak value of verticality increases for $0{\cdot}5 < \omega < 1{\cdot}2$. For $\omega > 1{\cdot}2$ the verticality decreases with increasing d_n except for the bottom curves for $d_n = 0{\cdot}8$, where the multiple solutions still exist. Verticality is insensitive to fluid drag at $\omega = 0{\cdot}47$ and $\omega = 1{\cdot}15$. The corresponding curves of the point mass radius x_d versus rotation speed are plotted in Figure 2(b). Solid, dotted, and dash-dotted lines signify stable, divergently unstable, and dynamically flutter unstable solutions, respectively. Generally, configurations with large point mass radius have small verticality and vice versa. Increasing rotation speed first increases and then decreases the point mass radius when d_n is not small. As d_n increases, the maximum

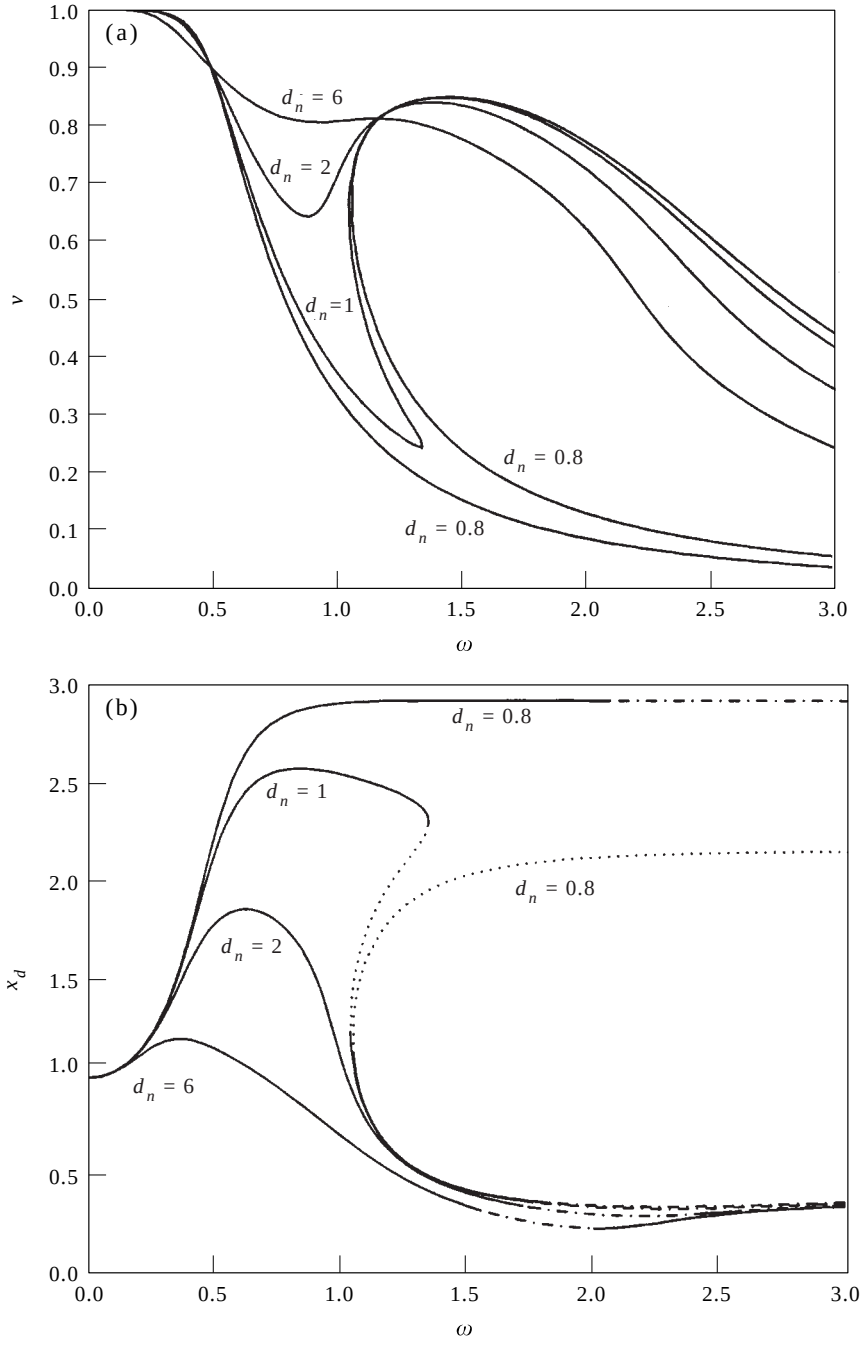

Figure 2. (a) Steady state verticality $v = h/l$ versus rotation speed ω for four d_n values. The system parameters are $l = 3$, $\gamma = 600$, $\rho = 1$, $d = 0{\cdot}1d_n$, and $m = w = 3{\cdot}5$. (b) Steady state point mass radius x_d versus rotation speed ω for four d_n values. Solid, dotted, and dashed-dotted curves represent stable, divergently unstable, and flutter unstable steady state solutions, respectively.

point mass radius decreases. As reported by Choo and Casarella [4], unique solutions exist for sufficiently large fluid drag. In all cases, however, there is a wide speed range with no stable solutions.

Figure 3 shows the root locus of the first two eigenvalues versus rotation speed for $d_n = 1$. At low speed (A), the eigenvalues are in the left half plane. The first eigenvalue decreases, becomes zero, and at B, the real part becomes positive. Between B and C the positive real eigenvalue signifies divergent instability. The solutions between C and D are stable as indicated by the root locus. When ω increases to 1·735 at point D, however, one of the eigenvalues crosses the imaginary axis and enters the right half plane. Thus, a Hopf bifurcation occurs and leads to flutter instability. The unstable eigenvalue is greater than the stable eigenvalue, indicating second mode flutter in the range (D–E). The solution curves for $d_n = 2$ and $d_n = 6$ in Figure 2(b) do not show second mode flutter in this speed range. The stability of the steady state configurations for $d_n = 0{\cdot}8$ is similar to that of $d_n = 1$ except that most configurations with large point mass radius lose stability by third mode flutter for $\omega > 2{\cdot}02$.

Experiments conducted by Russell and Anderson [6, 7] qualitatively verify the results. For small air drag, stable steady state configurations are obtained in the regions corresponding to AB and CD but not BC in Figure 3 (see Figure 4 of reference [6]). Multiple steady state solutions disappear when the air drag is large (e.g., $d_n \geqslant 2$ curves in Figure 2(b)). For $d_n = 6$, the stable regions corresponding to $0 < \omega < 1{\cdot}59$ and $3 \geqslant \omega > 2{\cdot}01$, and the flutter unstable region corresponding to $1{\cdot}59 < \omega < 2{\cdot}01$ in Figure 2(b) agree with the results shown in Figure 5.5 of reference [7].

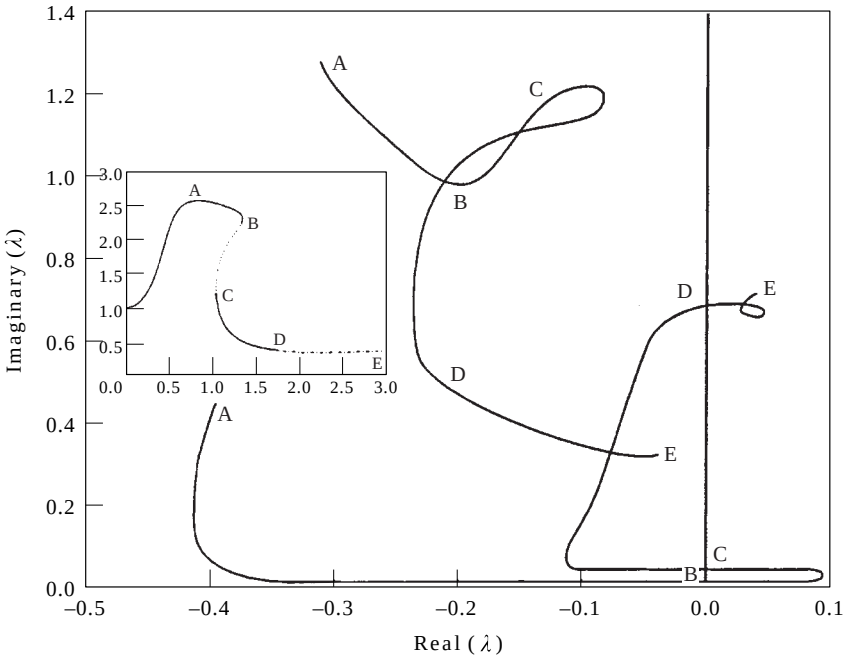

Figure 3. Root locus for the steady state solutions in Figure 2(b) with $d_n = 1$. For clarity, purely real roots are staggered with respect to the real axis.

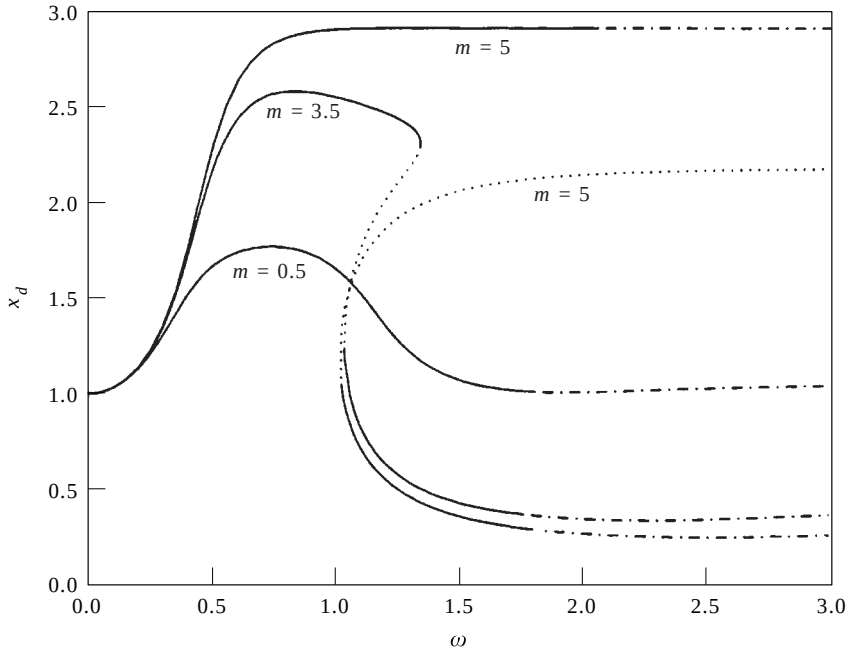

Figure 4. Steady state verticality $v = h/l$ versus rotation speed ω for three point mass values. Solid, dotted, and dashed-dotted curves represent stable, divergently unstable, and flutter unstable of the steady state solutions, respectively. The system parameters are $l = 3$, $\gamma = 600$, $\rho = 1$, $d = 0{\cdot}1$, $d_n = 1$, and $m = w$.

5.2. POINT MASS EFFECT

Second, the effect of the point mass on the steady state solutions is studied. Figure 4 shows point mass radius versus rotation speed for $l = 3$, $\gamma = 600$, $\rho = 1$, and $d_n = 1$.

Again, the solid curves represent stable solutions while the dotted and dash-dotted curves denote divergent and flutter instabilities, respectively. Note that both the steady state solutions and stability are similar to those in Figure 2(b). Therefore, increasing m with unchanged damping is similar to decreasing the fluid drag with constant tip mass.

5.3. CABLE LENGTH EFFECT

Finally, the effect of cable length is investigated with $\gamma = 600$, $\rho = 1$, $d_n = 1$ and $m = 3{\cdot}5$.

Figure 5(a) shows the verticality versus length for three rotation speeds. By increasing the length, the verticality decreases, increases, and then decreases again. Multiple jump phenomena appear at high rotation speeds. Figure 5(b) shows the point mass radius increasing, jumping or decreasing, and finally approaching zero with increasing length. Low rotation speed leads to stable single-valued solutions and high rotation speed results in multiple solutions with varied instabilities. Figure 6 plots the root locus of the first three eigenvalues for $\omega = 2{\cdot}5$. The system is stable from A to B, third mode flutter unstable from B to C, first mode divergent unstable from C to D, and second mode flutter unstable from D to E.

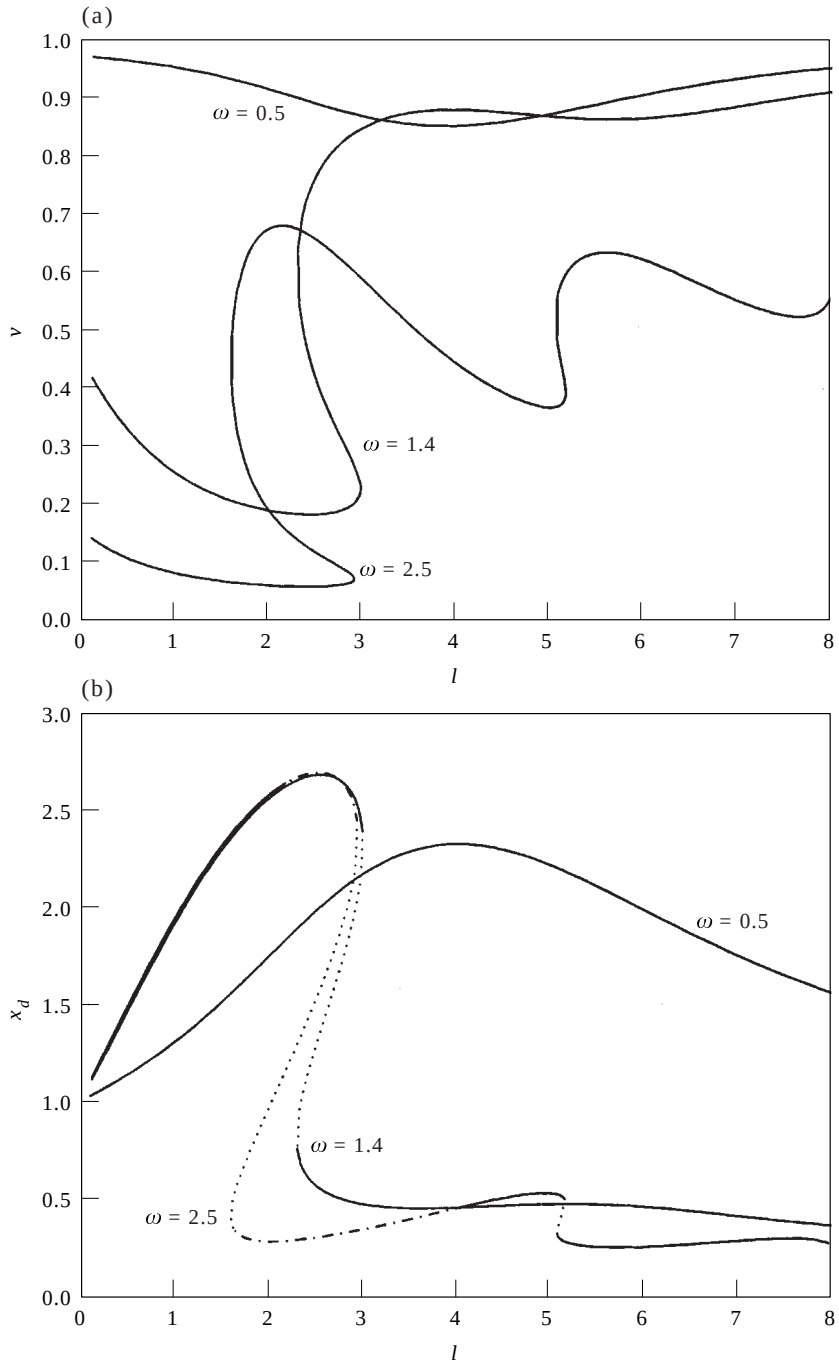

Figure 5. (a) Steady state verticality $v = h/l$ versus cable length l for three rotation speeds ω. The system parameters are $\gamma = 600$, $\rho = 1$, $d = 0{\cdot}1$, $d_n = 1$, and $m = w = 3{\cdot}5$. (b) Steady state point mass radius x_d versus cable length l for three rotation speeds ω. Solid, dotted, and dash-dotted curves represent stable, divergently unstable, and flutter unstable steady state solutions, respectively.

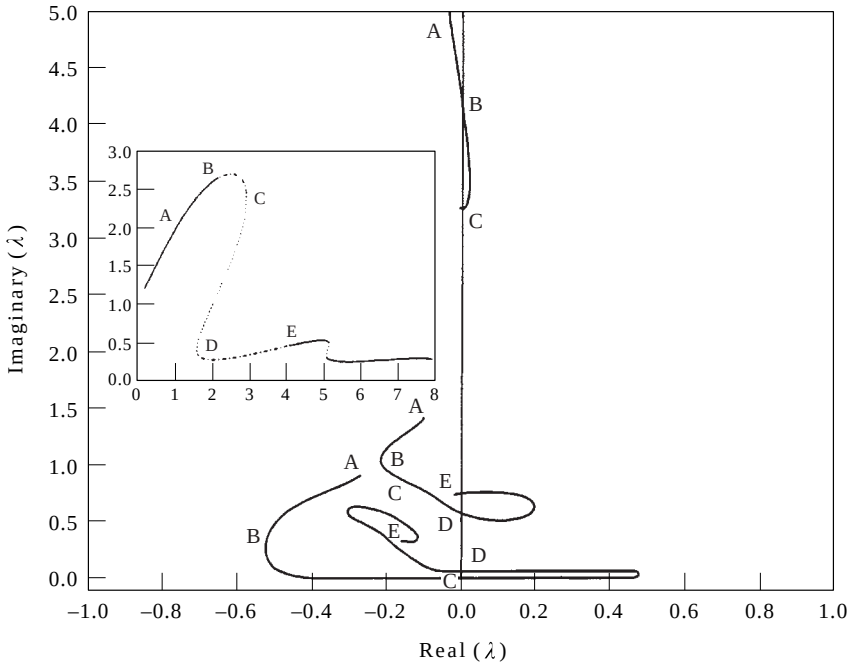

Figure 6. Root locus for the steady state solutions in Figure 5(b) with $\omega = 2{\cdot}5$. For clarity, purely real roots are staggered with respect to the real axis.

6. CONCLUSIONS

Multiple equilibrium solutions for a circularly towed cable–body system exist when the fluid drag is small, point mass is large, or rotation speed is high. Divergently unstable solutions lead to jump phenomena. High rotation speed causes Hopf bifurcations and second mode flutter for small point mass radius and third mode flutter for large point mass radius. Generally, increasing fluid drag increases the stable regions. Sufficiently low rotation speed ensures stable single-valued steady state solutions.

ACKNOWLEDGMENT

This research was supported in part by the U.S. Office of Naval Research.

REFERENCES

1. T. K. Caughey 1958 in *Proceedings of the Third U.S. National Congress of Applied Mechanics*, 61–108. Whirling of a heavy chain.
2. J. Huang 1969 *U.S. Navel Air Development Center Report NADC-AM*-6849. Mathematical model for long cable towed by orbiting aircraft.
3. R. A. Skop and Y. Choo 1971 *Journal of Aircraft* **8**, 856–862. The configuration of a Cable towed in a circular path.
4. Y. Choo and M. J. Casarella 1972 *Journal of Hydronautics* **6**, 51–57. Configuration of a towline attached to a vehicle moving in a circular path.

5. J. J. Russell and W. J. Anderson 1977 *International Journal of Non-Linear Mechanics* **12**, 91–101. Equilibrium and stability of a whirling rod–mass system.
6. J. J. Russell and W. J. Anderson 1977 *Journal of Aircraft* **14**, 680–686. Equilibrium and stability of a circularly towed cable subject to aerodynamic drag.
7. J. J. Russell 1974 *PhD Dissertation*, *University of Michigan*. Equilibrium and stability of a whirling cable.
8. F. Zhu, R. Sharma and C. D. Rahn 1997 *ASME Journal of Applied Mechanics* **64**(3). Vibrations of elastic ballooning strings.
9. F. Zhu, K. Hall and C. D. Rahn 1998 *International Journal of Non-linear Mechanics* **33**, 33–46. Steady state response and stability of ballooning strings in air.
10. M. Abramowitz and I. A. Stegun 1965 *Handbook of Mathematical Functions*. New York: Dover publications.

APPENDIX A: EXACT PLANAR STEADY STATE SOLUTION

Neglecting the cable weight in the fluid and the drag (i.e., $\rho = 0$ and $d_n = d = 0$) constrains the steady state solution to the x–z plane with

$$(px_{,s})_{,s} = -\omega^2 x, \qquad (pz_{,s})_{,s} = 0, \qquad p = p_d + \frac{\omega^2}{2}(x_d^2 - x^2). \tag{A1–A3}$$

The corresponding boundary conditions are

$$x(0) = x_d, \qquad z(0) = 0, \qquad x_{,s}(0) = -\omega^2 \frac{m x_d}{p_d}, \qquad z_{,s}(0) = \frac{w}{p_d}, \qquad x(l) = 1, \tag{A4}$$

with

$$p_d = \sqrt{\omega^4 m^2 x_d^2 + w^2}. \tag{A5}$$

Elimination of s from equations (A1) and (A2) gives

$$\frac{\mathrm{d}z}{\mathrm{d}x} = \frac{C}{\sqrt{p^2 - C^2}}, \tag{A6}$$

where C is an integration constant. From equation (A4),

$$\frac{\mathrm{d}z(0)}{\mathrm{d}x} = -\frac{w}{\omega^2 m x_d} = \frac{C}{\sqrt{p_d^2 - C^2}},$$

and, using equation (A5),

$$C = -w. \tag{A7}$$

Transformation of

$$\bar{x} = \frac{x}{\sqrt{2(p_d + 0{\cdot}5 x_d^2 \omega^2 - C)}} \qquad \text{and} \qquad \bar{z} = \frac{\sqrt{p_d + 0{\cdot}5 x_d^2 \omega^2 + C}}{\sqrt{2}C} z \tag{A8}$$

in equation (A6) gives

$$\frac{\mathrm{d}\bar{z}}{\mathrm{d}\bar{x}} = \frac{1}{\sqrt{(1 - \bar{x}^2)(1 - k^2 \bar{x}^2)}}, \tag{A9}$$

where

$$k^2 = \frac{p_d + 0{\cdot}5x_d^2\omega^2 - C}{p_d + 0{\cdot}5x_d^2\omega^2 + C}. \tag{A10}$$

Integration of equation (A9) yields

$$\bar{z} = \int_0^{\bar{x}} \frac{\mathrm{d}\bar{x}}{\sqrt{(1-\bar{x}^2)(1-k^2\bar{x}^2)}},$$

or

$$\bar{x} = \mathrm{sn}\,(\bar{z}). \tag{A11}$$

where sn is the Jacobian elliptical sine function [10]. The boundary conditions $x = 1$ and $z = H/a = h$ at $s = l$ provide

$$l = \int_0^h \sqrt{1 + \frac{1}{C^2}(p_d + 0{\cdot}5x_d^2\omega^2 + C)(p_d + 0{\cdot}5x_d^2\omega^2 - C)\left[\frac{\mathrm{d}(\mathrm{sn}\,(\bar{z}))}{\mathrm{d}\bar{z}}\right]^2}\,\mathrm{d}z, \tag{A12}$$

$$\frac{1}{\sqrt{2(p_d + 0{\cdot}5x_d^2\omega^2 - C)}} = \mathrm{sn}\left(\frac{\sqrt{p_d + 0{\cdot}5x_d^2\omega^2 + C}}{\sqrt{2}C}\,h\right). \tag{A13}$$

Solution of equations (A12) and (A13) gives h and x_d. The cable steady state configurations are calculated from equation (A11).

APPENDIX B: JACOBIAN MATRIX

In equation (17), $\mathbf{v}_n^f$ can be expressed as

$$\mathbf{v}_n^f = \mathbf{v}_n^i + \mathbf{v}_n, \tag{B1}$$

where $\mathbf{v}_n^i$ is defined by equation (27) and equation (B1) defines $\mathbf{v}_n$.

Linearization of the air drag force produces

$$d_n|\mathbf{v}_n^f|\mathbf{v}_n^f = d_n(|\mathbf{v}_n^i|\mathbf{v}_n^i + \mathbf{J}\mathbf{v}_n),$$

where the Jacobian Matrix is

$$\mathbf{J} = \frac{\partial(|\mathbf{v}_n^f|\mathbf{v}_n^f)}{\partial \mathbf{v}_n^f}\bigg|_{\mathbf{v}_n = 0} = \begin{bmatrix} J_1 & J_2 & J_3 \\ J_2 & J_4 & J_5 \\ J_3 & J_5 & J_6 \end{bmatrix} = |\mathbf{v}_n^i|\mathbf{I} + \frac{1}{|\mathbf{v}_n^i|}\begin{bmatrix} x_1^2 & x_1x_2 & x_1x_3 \\ x_1x_2 & x_2^2 & x_2x_3 \\ x_1x_3 & x_2x_3 & x_3^2 \end{bmatrix},$$

and

$$x_1 = -y + x_{,s}(yx_{,s} - y_{,s}x), \qquad x_2 = x - y_{,s}(xy_{,s} - x_{,s}y), \qquad x_3 = z_{,s}(yx_{,s} - y_{,s}x),$$

$$|\mathbf{v}_n^i| = \sqrt{x_1^2 + x_2^2 + x_3^2},$$

and $\mathbf{I}$ is the unit matrix.

To calculate $\mathbf{J}_d$, one has

$$\mathbf{v}_d^f = \mathbf{v}_d^i + \mathbf{v}_d,$$

where

$$\mathbf{v}_d^i = \mathbf{k} \times \mathbf{r} \qquad \text{and} \qquad \mathbf{v}_d = \frac{\partial \mathbf{u}}{\partial t} + \mathbf{k} \times \mathbf{u}.$$

Hence,

$$\mathbf{J}_d = \frac{\partial (|\mathbf{v}_d^f| \mathbf{v}_d^f)}{\partial \mathbf{v}_d^f}\bigg|_{\mathbf{v}_d = 0} = \sqrt{y^2 + x^2}\mathbf{I} + \frac{1}{\sqrt{y^2 + x^2}} \begin{bmatrix} y^2 & -xy & 0 \\ -xy & x^2 & 0 \\ 0 & 0 & 0 \end{bmatrix}.$$

At $s = 0$, $y = 0$, $x = x_d$, one has

$$\mathbf{J}_d = \begin{bmatrix} x_d & 0 & 0 \\ 0 & 2x_d & 0 \\ 0 & 0 & x_d \end{bmatrix}.$$

APPENDIX C: MATRIX OPERATORS

In equation (40), $\mathbf{G}$ is defined as

$$\mathbf{G} = (\mathbf{G}_0 + d_n \mathbf{D}),$$

where

$$\mathbf{G}_0 = \begin{bmatrix} 0 & -2 & 0 \\ 2 & 0 & 0 \\ 0 & 0 & 0 \end{bmatrix},$$

$$\mathbf{D}(1, 1) = -J_2 x_{,s} y_{,s} + J_1 y_{,s}^2 + J_1 z_{,s}^2 - J_3 x_{,s} z_{,s},$$

$$\mathbf{D}(1, 2) = -J_3 y_{,s} z_{,s} + J_2 z_{,s}^2 + J_2 x_{,s}^2 - J_1 y_{,s} x_{,s},$$

$$\mathbf{D}(1, 3) = J_3 y_{,s}^2 - J_2 z_{,s} y_{,s} - J_1 z_{,s} x_{,s} + J_3 x_{,s}^2,$$

$$\mathbf{D}(2, 1) = J_2 z_{,s}^2 + J_2 y_{,s}^2 - J_4 x_{,s} y_{,s} - J_5 x_{,s} z_{,s},$$

$$\mathbf{D}(2, 2) = -J_5 y_{,s} z_{,s} - J_2 x_{,s} y_{,s} + J_4 z_{,s}^2 + J_4 x_{,s}^2,$$

$$\mathbf{D}(2, 3) = -J_4 z_{,s} y_{,s} + J_5 y_{,s}^2 + J_5 x_{,s}^2 - J_2 z_{,s} x_{,s},$$

$$\mathbf{D}(3, 1) = -J_5 x_{,s} y_{,s} - J_6 x_{,s} z_{,s} + J_3 y_{,s}^2 + J_3 z_{,s}^2,$$

$$\mathbf{D}(3, 2) = -J_6 y_{,s} z_{,s} - J_3 y_{,s} x_{,s} + J_5 x_{,s}^2 + J_5 z_{,s}^2,$$

$$\mathbf{D}(3, 3) = -J_3 x_{,s} z_{,s} - J_5 y_{,s} z_{,s} + J_6 y_{,s}^2 + J_6 x_{,s}^2.$$

The matrix operator $\mathbf{K}$ is

$$\mathbf{K} = \mathbf{K}_0 + (\mathbf{K}_s + d_n \mathbf{K}_{s0}) \frac{\partial}{\partial s} + \mathbf{K}_{ss} \frac{\partial^2}{\partial s\, \partial s},$$

where

$$\mathbf{K}_0(1, 1) = -1 + d_n(J_2 x_{,s}^2 + J_2 z_{,s}^2 - J_3 y_{,s} z_{,s} - J_1 y_{,s} x_{,s}),$$

$$\mathbf{K}_0(1, 2) = d_n(J_2 x_{,s} y_{,s} - J_1 z_{,s}^2 + J_3 x_{,s} z_{,s} - J_1 y_{,s}^2),$$

$$\mathbf{K}_0(2, 1) = d_n(-J_5 y_{,s} z_{,s} - J_2 x_{,s} y_{,s} + J_4 z_{,s}^2 + J_4 x_{,s}^2),$$

$$\mathbf{K}_0(2, 2) = -1 + d_n(J_5 x_{,s} z_{,s} - J_2 y_{,s}^2 - J_2 z_{,s}^2 + J_4 x_{,s} y_{,s}),$$

$$\mathbf{K}_0(3, 1) = d_n(-J_6 y_{,s} z_{,s} - J_3 y_{,s} x_{,s} + J_5 x_{,s}^2 + J_5 z_{,s}^2),$$

$$\mathbf{K}_0(3, 2) = d_n(-J_3 z_{,s}^2 + J_6 x_{,s} z_{,s} + J_5 x_{,s} y_{,s} - J_3 y_{,s}^2),$$

$$\mathbf{K}_0(1, 3) = 0, \qquad \mathbf{K}_0(2, 3) = 0, \qquad \mathbf{K}_0(3, 3) = 0,$$

$$\mathbf{K}_s = \frac{1}{\omega^2} \begin{bmatrix} -p_{,s} - 2\gamma x_{,s} x_{,ss} & -\gamma(x_{,s} y_{,ss} + x_{,ss} y_{,s}) & -\gamma(x_{,s} z_{,ss} + x_{,ss} z_{,s}) \\ -\gamma(x_{,s} y_{,ss} + x_{,ss} y_{,s} & -p_{,s} - 2\gamma y_{,s} y_{,ss} & -\gamma(y_{,s} z_{,ss} + y_{,ss} z_{,s}) \\ -\gamma(x_{,s} z_{,ss} + x_{,ss} z_{,s}) & -\gamma(y_{,s} z_{,ss} + y_{,ss} z_{,s}) & -p_{,s} - 2\gamma z_{,s} z_{,ss} \end{bmatrix},$$

$$\mathbf{K}_{s0}(1, 1) = 2J_2 x x_{,s} + J_3 y z_{,s} - J_1 y_{,s} x + J_2 y y_{,s},$$

$$\mathbf{K}_{s0}(1, 2) = -2J_1 y y_{,s} - J_1 x x_{,s} + J_2 x_{,s} y - J_3 x z_{,s},$$

$$\mathbf{K}_{s0}(1, 3) = -2J_1 y z_{,s} + J_3 x_{,s} y - J_3 y_{,s} x + 2J_2 x z_{,s},$$

$$\mathbf{K}_{s0}(2, 1) = J_4 y y_{,s} + 2J_4 x x_{,s} - J_2 y_{,s} x + J_5 y z_{,s},$$

$$\mathbf{K}_{s0}(2, 2) = -J_2 x x_{,s} + J_4 x_{,s} y - J_5 x z_{,s} - 2J_2 y y_{,s},$$

$$\mathbf{K}_{s0}(2, 3) = -J_5 y_{,s} x + J_5 x_{,s} y - 2J_2 y z_{,s} + 2J_4 x z_{,s},$$

$$\mathbf{K}_{s0}(3, 1) = -J_3 y_{,s} x + J_5 y y_{,s} + 2J_5 x x_{,s} + J_6 y z_{,s},$$

$$\mathbf{K}_{s0}(3, 2) = -J_3 x x_{,s} - J_6 x z_{,s} - 2J_3 y y_{,s} + J_5 x_{,s} y,$$

$$\mathbf{K}_{s0}(3, 3) = -2J_3 y z_{,s} + 2J_5 x z_{,s} - 2J_6 y_{,s} x + J_6 x_{,s} y,$$

$$\mathbf{K}_{ss} = \frac{1}{\omega^2} \begin{bmatrix} -\gamma x_{,s}^2 - p & -\gamma x_{,s} y_{,s} & -\gamma x_{,s} z_{,s} \\ -\gamma x_{,s} y_{,s} & -\gamma y_{,s}^2 - p & -\gamma y_{,s} z_{,s} \\ -\gamma x_{,s} z_{,s} & -\gamma y_{,s} z_{,s} & -\gamma z_{,s}^2 - p \end{bmatrix}.$$

Finally, $\mathbf{G}_d$ and $\mathbf{K}_d$ are given by

$$\mathbf{G}_d = \frac{1}{m} \begin{bmatrix} \mathrm{d}x_d & -2m & 0 \\ 2m & 2\,\mathrm{d}x_d & 0 \\ 0 & 0 & \mathrm{d}x_d \end{bmatrix},$$

$$\mathbf{K}_d = \mathbf{K}_{do} + \mathbf{K}_{ds} \frac{\partial}{\partial s},$$

where

$$\mathbf{K}_{do} = \frac{1}{m}\begin{bmatrix} -m & -\mathrm{d}x_d & 0 \\ 2\,\mathrm{d}x_d & -m & 0 \\ 0 & 0 & 0 \end{bmatrix},$$

$$\mathbf{K}_{ds} = \frac{1}{m\omega^2}\begin{bmatrix} -\gamma x_{,s}^2 - p & -\gamma x_{,s}y_{,s} & -\gamma x_{,s}z_{,s} \\ -\gamma x_{,s}y_{,s} & -\gamma y_{,s}^2 - p & -\gamma y_{,s}z_{,s} \\ -\gamma x_{,s}z_{,s} & -\gamma y_{,s}z_{,s} & -\gamma z_{,s}^2 - p \end{bmatrix}\Bigg|_{s=0}.$$

APPENDIX D: COMPARISON FUNCTIONS

Consider the constant tension cable equation

$$p_d u_{,ss} = u_{,tt}, \tag{D1}$$

subjected to the boundary conditions

$$u(l,t) = 0 \qquad \text{and} \qquad p_d u_{,s}(0,t) = m u_{,tt}(0,t). \tag{D2}$$

The assumed solution

$$u = \sin\left(\beta \frac{l-s}{l}\right) \mathrm{e}^{i\alpha t} \tag{D3}$$

yields a frequency equation

$$\cos\beta = m\frac{\beta}{l}\sin\beta \tag{D4}$$

with an infinite number of solutions β_i. The comparison functions used in equation (41) are

$$\theta_j(s) = \sin\left(\beta_j \frac{l-s}{l}\right). \tag{D5}$$